symmetry

MDPI

Article

Computational Modeling of Thermodynamical Pulsatile Flow with Uncertain Pressure in Hydrocephalus

Hemalatha Balasundaram [1], Nazek Alessa [2,*], Karuppusamy Loganathan [3,*], V. Vijayalakshmi [4] and Nayani Uday Ranjan Goud [5]

[1] Vels Institute of Science, Technology and Advance Studies, Chennai 600117, Tamilnadu, India
[2] Department of Mathematical Sciences, College of Sciences, Princess Nourah Bint Abdulrahman University, P.O. Box 84428, Riyadh 11671, Saudi Arabia
[3] Department of Mathematics and Statistics, Manipal University Jaipur, Jaipur 303007, Rajasthan, India
[4] Department of Science and Humanities, Karpagam Academy of Higher Education, Coimbatore 641021, Tamilnadu, India
[5] Department of Aeronautical Engineering, MLR Institute of Technology, Hyderabad 500043, Telangana, India
* Correspondence: nazekaa@yahoo.com (N.A.); loganathankaruppusamy304@gmail.com (K.L.)

Abstract: The watery cerebrospinal fluid that flows in the subarachnoid space (SAS) surrounds the entire central nervous system via symmetrical thermo-solute flow. The significance of this study was to present a flexible simulation based on theoretical vivo inputs onto a mathematical framework to describe the interaction of cerebrospinal fluid circulation restricted to a pathological disorder. The pathophysiology disorder hydrocephalus is caused by an enormous excess of asymmetric fluid flow in the ventricular region. This fluid imposition increases the void space of its boundary wall (Pia mater). As a result, the dumping effect affects an inertial force in brain tissues. A mathematical model was developed to impose the thermal dynamics of hydrocephalus, in which solute transport constitutes the excess watery CSF fluid caused by hydrocephalus, in order to demonstrate perspective changes in ventricular spaces. This paper investigated brain porous spaces in order to strengthen the acceleration and thermal requirements in the CNS mechanism. To characterize neurological activities, a unique mathematical model that includes hydrodynamics and nutrient transport diffusivity was used. We present the analytical results based on physical experiments that use the novel Laplace method to determine the nutrients transported through permeable pia (brain) parenchyma with suitable pulsatile boundary conditions. This causes high CSF pressure and brain damage due to heat flux over the SAS boundary wall. As a result of the increased Schmidt number, the analysis of the hydrocephalus problem revealed an increase in permeability and drop in solute transport. A high-velocity profile caused a rise in thermal buoyancy (Grashof number). When the CSF velocity reached an extreme level, it indicated a higher Womersley number. Additionally, the present study compared a number of clinical studies for CSF amplitude and pressure. We validated the results by providing a decent justification with the clinical studies by appropriate field references.

Keywords: cerebrospinal fluid disorder; hydrocephalus; heat transfer; inlet pulsatile flow velocity; pia mater; intracranial pressure (ICP); Laplace transform

Citation: Balasundaram, H.; Alessa, N.; Loganathan, K.; Vijayalakshmi, V.; Goud, N.U.R. Computational Modeling of Thermodynamical Pulsatile Flow with Uncertain Pressure in Hydrocephalus. *Symmetry* **2023**, *15*, 534. https://doi.org/10.3390/sym15020534

Academic Editors: Ranjit Kumar Upadhyay and Ramalingam Udhayakumar

Received: 12 January 2023
Revised: 22 January 2023
Accepted: 31 January 2023
Published: 16 February 2023

1. Introduction

The brain and spinal cord as well as cerebrospinal fluid are part of the central nervous system (CNS). CSF is a watery fluid secreted by ventricles of the choroid plexus and flows around the cranium. It acts as a conduit for the transfer of nutrients and neuroendocrine substances that remove waste from the brain. It protects the brain from shock absorbers and external injury damage. Hydrocephalus is an abnormal syndrome in which excess CSF accumulates in the ventricular regions. Hydrocephalus disrupts the flow of fluid in the ventricular regions, causing disruptions in production and circulation. These changes in hydrocephalic CSF cause a significant change in intracranial pressure, resulting in shunting in

the central nervous system. The objective of this research was to focus on diffusive transport due to temperature variations with appropriate pulsatile outlet boundary conditions. The mathematical modeling of this accumulation results in the geometrical pathophysiological syndrome hydrocephalus.

There are many research articles in CSF relating pulsatile flow with appropriate boundary conditions. According to the mechanics of the cranial system, it is not easy to solve the computational method without proper governing equations. In individuals with hydrocephalus of diverse etiologies, Hirashima et al. [1] documented the cerebral temperature estimated at various heights beneath the pia mater. For all instances, they noticed that the temperature grew progressively and thoroughly, along with the ventricles exhibiting the maximum temperature. Rajasekaran et al. [2] evaluated the CSF flow frequency in hydrocephalus bypasses using an improved shunt tubular structure with a layer on top. In addition to performing a FEM simulation of the shunt system's fluid and thermal behavior, they determined the acceleration and its flow rate by segregating the performance of temperature acquired in various periods with two sampling locations. Using meninges temperature monitoring from a CSF layer, Madsen [3] developed a novel quasi-technique to simulate CSF fluid flow in a hollow tube in hydrocephalic patients (ShuntCheck). A statistical examination of 100 suspected shunt malfunctions was also conducted, and only a very few of these required more surgical examination. By monitoring non-invasive endovascular heat convection CSF shunted flow, Neff [4] improved neuroimaging techniques and radioactivity shunt research. Leszek Herbowsk [5] provided a thermodynamic method for cerebrospinal fluid circulation by using Brownian motion and gravity force for cerebrospinal fluid bulk flow that was oriented upward and downward, respectively.

Linninger, A. et al. [6] illustrated a bulk flow in the intracranial CSF flow dynamics related to vascular pulsations. They provided a comprehensive discussion of CSF conditions such as type-1 Chiari malformation, syringomyelia, hydrocephalus, and cerebri pseudotumor. The mechanics of the CSF and blood were extensively examined by using a mathematical model for CSF dynamics that had been constructed.

The cerebrum in different heat flux changes with high tissue metabolic rate and thermally protected cranium, according to Donnelly, Joseph, and Marek Czosnyka [7], identified no high-volume bloodstream to cool and settle the higher-than-normal cerebrum temperature. The temperature of brain tissue is usually cooler than that of penetrating blood vessels, and the temperature of upwelling blood veins is cooler compared to that of the blood vessels. Thus, cerebral blood pressure might be regarded as a conscious factor. Gholampour et al. [8] provided 3-dimensional hydro elastic computational modeling of an interface between CSF and the brain tissue of subjects with hydrocephalus during shunting. Hydrocephalus patients were found to have significantly increased CSF average pressure and mean fluid velocity compared with healthy people, at least in non-communicating hydrocephalus. A quasi-second law (stochastic) thermodynamic model has been developed by Zakharov and Sadovsky [9] to explain how circulating blood helps thermoregulation organisms balance physiological body temperatures. Their simulation showed a clear correlation between skin temperature and environmental temperatures.

Diffusion tensor imaging was used by Keong et al. [10] to assess the surface features and reproducibility of white deeper vessels found in the brain, which are damaged during atmospheric pressure before and immediately after the shunt. According to James et al. [11], the development of a training session for people with hydrocephalus should be carefully planned with potential consequences in mind. The current position of hydrocephalus inquiry and therapy was formed as a result of an excessive CSF influence. Hydrocephalus was researched by Smillie [12], who described a pathological situation that seems to be comparable to clinical observations.

In order to simulate and monitor CSF hydro-dynamics for healthy individuals as well as hydrocephalic patients, Zhu [13] developed quantitative MRI techniques. Reconstructed geometric models were demonstrated by Ying Hsu et al. [14] to calculate the nanoparticles' impacts on CSF flow mechanics and the rate of flow throughout CNS. They demonstrated

how nerve roots and trabeculae produce intricate domains with microvasculature along the spine and how pulsatile flow surrounding microanatomy-induced vortices enhances medication dispersion. In order to replicate the kinematic interface in quasi hydrocephalus (NCH) geometries, Gholampour [15] developed ADINA computational geometry software to demonstrate the assessment process of the ventricular space and pressure of CSF, where the one that controls the hydro-dynamic features that characterize circulation and increases the CSF pressure is the most serious parameter in neurological symptoms. Additionally, it can determine the degree of the CSF pulsate and the sequence lag between both the flow rate and pressure gradient functions. The brain tissue in people with hydrocephalus and in healthy participants was described in [16]. By specifying inlet boundary conditions with different constant pressures for healthy and diseased humans, they went ahead. Medical imaging is used to determine the absolute value of intracranial pressure without using MRI analysis. Even though computing CSF pressure using a CFD model is uncertain and cannot be carried out without error, they used an analytical method to obtain the precise value. The pressure is unknown in the model's biphasic approach simulation.

Most researchers in a variety of disciplines, particularly engineering and biology, have developed a model that connects the momentum and transport diffusivity of various fluids in disorder with various methods (Table 1). Neurologists have described pathological conditions of the brain and central nervous system both theoretically and practically. Biofluid scientists have investigated the unusual event of CSF thermos-dynamic behavior. For the disorder of congenital hydrocephalus, Balasundaram et al. [17] developed a mathematical simulation of ventricular elasticity. Hetnarski [18] provided an illustration of the conventional Laplace and inverse transform together with its error and its error complementary function. Gholampour [19,20] examined the changes in the disease's numerous physiological and physical characteristics before the therapeutic procedure for individuals with communicating and non-communicating hydrocephalus. Lininger et al. [21] illustrated a bulk flow in the intracranial CSF flow dynamics that related to vascular pulsations. They provided a comprehensive discussion of CSF conditions such as type-1 Chiari malformation, syringomyelia, hydrocephalus, and cerebral pseudotumor. The mechanics of the CSF and blood were extensively examined using a mathematical model for CSF dynamics that had been constructed. Sweetman et al. [22] simulated the fluid–structure interaction between the brain tissues and CSF hydrodynamical flow across non-communicating hydrocephalus and healthy patients, while Lininger et al. [23] demonstrated that the aqueduct CSF volume is accessible when simulating hydrocephalus patients. They used available clinical study reports to provide the treatment process, which will act as a shunt-responder to predict the patients from the shunt. Taylor et al. [24] generated a two-dimensional cranial model for patients suffering from hydrocephalus malignancy. Cheng, Shaokoon, et al. [25] suggested using a numerical analysis like the finite-element method with the pressure of CSF as the boundary conditions. The geometry of the ventricular system with brain tissue is extremely complicated, which has a significant impact on problem-solving scenarios. To fulfill the requirements of geometrical complexity, three-dimensional simulation was used to explore the kinematics of hydrocephalus. Hochstetler et al. [26] proposed a genetic explanation for hydrocephalic CSF flow to account for the putative prediction of ventricular deformation by pulsatile potential vanilloid 4 receptors. These have been supported by the osmotic balance, mediator parenchyma, change in pressure, and skin temperature of the CSF flow boundary.

Due to the pressure–volume fluctuations in patients with hydrocephalus syndrome and non-patients, Eide and Brean [27] built a model and demonstrated that the model they constructed revealed a reasonable shift in the records of patients experiencing hydrocephalus. Gholampour [28] looked beyond the inlet or outlet boundary conditions and found that the interface between fluid and solid models is an important boundary condition parameter in various solution techniques such as CFD and FSI. [29] Lefever et al. studied a biphasic model that was used to represent the brain tissue of a patient with non-communicating hydrocephalus. According to Taher and Gholampour [30], the interface between the interior and exterior layers of the sub-arachnoid layer (SAS) is a

boundary of the FSI and the boundary of SAS with the no-slip boundary condition. The fluid flow momentum was computed using coupled governing equations. Safaei et al. [31] discussed how temperature-induced turbulent flow affects nanoparticle solute transport. They also included nanoparticle molecules in the Reynolds number effects. Wilkie et al. [32] demonstrated the physiology of brain tissue in individuals with healthy and hydrocephalus patients influenced by gender and age, which had a significant impact on the outcomes of the biomechanical simulations. As a result, the current study's selection of healthy individuals and patients had significant limitations. Miller et al. [33] conducted an empirical study on a complicated and significant model based on the FSI border that distinguished the brain parenchyma from the ventricular circulation and the cranium.

Table 1. Various solution methods used by some research publications.

Authors	Model Used	Source
Sweetman, Brian, and Andreas A. Linninger	Modeled using Fourier series and used finite element method (FEM)	[22]
Eide, Per K., and Are Brean	Clinical and radiology simulation	[27]
Taher, Mehran, and Seifollah Gholampour	FSI method	[30]
Gholampour, Seifollah	Statistical and FSI method	[16]
Wilkie, K. P., C. S. Drapaca, and S. Sivaloganathan	Fractional Zener model (FZM)	[32]
Taylor, Zeike, and Karol Miller	Finite element method (FEM)	[24]
Lefever, Joel A., José Jaime García, and Joshua H. Smith	Finite element method (FEM)	[29]
Gholampour, Seifollah, and Nasser Fatouraee	Fluid–structure interaction (FSI) and CFD with three boundary conditions.	[15]

As a result of the interplay between the thermal solid model and the motion of the CSF caused by the hydrocephalus flowing within the spinal canal, we included an elastic effect in the current work. In other words, using an analytical method, we developed a novel model on CSF flow considering the effects of wall temperature in the presence of transport diffusivity, which resulted in enormous pressure change leading to severe medication therapy. To demonstrate CSF flow, many researchers have evaluated the system with numerous compartments and developed the geometry as a cylindrical tube due to the complexity of the flow in the cranial system. We defined the physical flow in Figure 1 as a closed cylindrical model through which the flow was generated by considering these compartments.

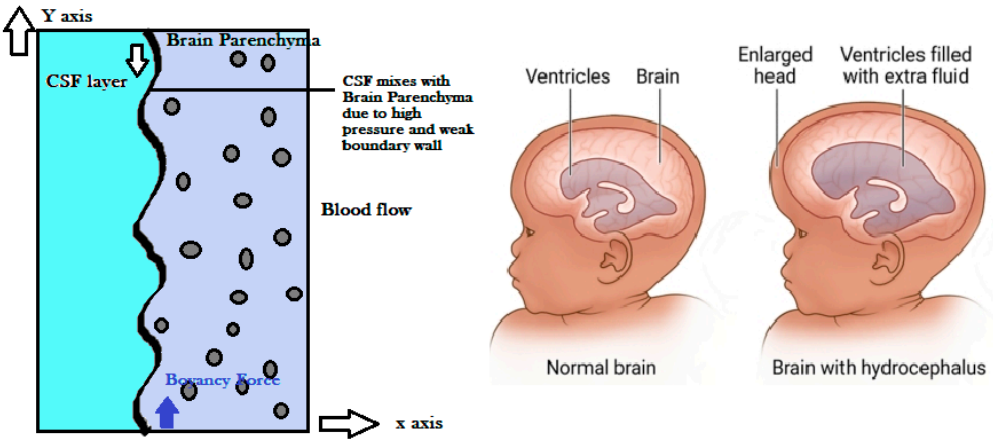

Figure 1. Flow configuration of CSF flow.

2. Formulation of the Problem

CSF, typically a translucent fluid that runs through the brain stem and central nervous system, protects the brain. Henceforth, CSF acts as a buoyancy force for the brain in which the fluid varies with respect to its density. The maximum volume of CSF is secreted by the foremost ventricle layer next to the pia mater. The CSF syndrome hydrocephalus produces excess fluid than that required and flows enormously in subarachnoid space, so we assumed that the flow of CSF is a Newtonian iso-thermal and in-compressible fluid. Despite the general dynamical model, we developed a fluid dynamical model for cerebrospinal fluid pulsatile flow with oscillating pressure variation with respect to time.

As the CSF acts as a buoyancy force for the brain, the Boussinesq approximation was used with the brain parenchyma. In this paper, we proposed a model based on the theory illustrated in [32], considering the boundary as the outer surface of the brain pia mater and inner layer, as the subarachnoid space was CSF flows and no slip in the inlet boundary flowing in a pulsatile nature. Taking the cartesian coordinate system $(x,\ y)$, where x lies along the center of the channel, y is the distance measured in the normal section. The fluid continues to maintain negligible on the surface of the sub-arachnoid space, fixed at the temperature ${T_w}^*$ and concentration ${C_w}^*$ higher than that of the room temperature and concentration as T_∞, C_0. Other properties of the CSF fluid mechanics were assumed to be constant. To simplify the examination of various parameters, certain assumptions were made:

i. The forces exerted in the fluid layer internally were taken as consistent excluding the density fluctuation in the buoyancy terminals;
ii. The pressure expelled in CSF flow due to hydrocephalus therefore flowed steadily;
iii. The subarachnoid space was bounded by a porous medium known as brain parenchyma;
iv. The porous medium for the pia mater was isotropic and homogeneous;
v. Steady-state circulation with hydrodynamic temperature and mass dispersion in the porous parenchyma was taken into consideration;
vi. Limiting the magnitude of the brain fluid's electro-magnetic account of the above presumptions, the governing equations for fluid movement, assuming a boundary layer and the Boussinesq approximation, the CSF flow can be depicted as below.

$$\frac{\partial {u_h}^*}{\partial x^*} + \frac{\partial {v_h}^*}{\partial y^*} = 0 \tag{1}$$

$$\frac{\partial {u_h}^*}{\partial t^*} = -\frac{1}{\rho}\frac{\partial {P_h}^*}{\partial x^*}\ p_k + \nu\left(\frac{\partial^2 {u_h}^*}{\partial {y^*}^2}\right) + g\beta_T({T_h}^* - {T_\infty}^*) - \frac{\nu}{{k_m}^*}{u_h}^* \tag{2}$$

$$\left(\frac{\partial {T_h}^*}{\partial t^*}\right) = \frac{k_T}{\rho C_p}\left(\frac{\partial^2 {T_h}^*}{\partial {y^*}^2}\right) - J({T_h}^* - {T_\infty}^*) \tag{3}$$

$$\left(\frac{\partial {C_h}^*}{\partial t^*}\right) = D\left(\frac{\partial^2 {C_h}^*}{\partial {y^*}^2}\right) - K{C_h}^* \tag{4}$$

$$\begin{gathered} {u_h}^* = 0\ ,\ {C_h}^* = {C_\infty}^*\ and\ {T_h}^* = {T_\infty}^*\ for\ y^* \geq 0, x^* > 0, t^* \leq 0 \\ {u_h}^* = u_0(1 + cos\omega t^*)\ ,\ {C_h}^* = {C_w}^*,\ {T_h}^* = {T_w}^*\ at\ y^* = 0 \\ {u_h}^* = 0, {C_h}^* \to {C_\infty}^*\ and\ {T_h}^* = {T_\infty}^*\ at\ y^* \to \infty,\ t^* > 0 \end{gathered} \tag{5}$$

Introducing dimensionless quantities, which are defined as follows:

$$u_h = \frac{{u_h}^*}{U_0}\ ,\ x = \frac{x^*}{l}\ ,y = \frac{y^* U_0}{\nu},\ {\theta_h}^* = \frac{{T_h}^* - {T_\infty}^*}{{T_w}^* - {T_\infty}^*}\ C^* = \frac{{C_h}^* - {C_\infty}^*}{{C_w}^* - {C_\infty}^*},\ P = \frac{{P_h}^*}{\rho {U_0}^2}\ \ t = \frac{t^* {U_0}^2}{\nu} \tag{6}$$

where ${u_h}^*,\ {T_h}^*, {C_h}^*, {P_h}^*$ denote the components that are dimensions of the cerebrospinal fluid flow velocity, energy, concentration, and pressure, respectively. x^*, y^*, t^* denote the dimensional coordinates and time variation; g depicts the fluid acceleration due to gravity; β_h and β_T denote the concentration coefficient and heat expansion; ${C_w}^*$ and ${T_w}^*$ represent

the wall concentration and wall temperature; $T_\infty{}^*$ denotes the prevailing temperature; t is the dimensionless time taken for CSF circulation; C_p represents the specific heat of fluid.

D indicates the diffusivity coefficient. u_h, C_h, θ_h depict the dimensionless velocity of the fluid flow, solute concentration, and temperature, respectively. U_0 denotes the characteristic velocity of the CSF fluid. P_h and p_k are the dimensionless pressure and permeability of brain parenchyma. ω^* represents the dimensionless angular velocity. $\propto^2$ represents the Womersley number, which quantifies the transient flow of the CSF. Furthermore, the flow rate of CSF will exceptionally increase the pressure, which varies exceptionally, so we assumed the pressure increases exponentially with respect to time. Henceforth, we developed a model relating the oscillating pressure variation for the CSF fluid flow.

$$\frac{\partial u_h}{\partial t} = -\frac{\partial P_h}{\partial x}\, p_k + \left(\frac{\partial^2 u_h}{\partial y^2}\right) - \sigma^2 u_h + \frac{G_{pv}}{Re^2} u_h + Gr\, \theta_h + Gc\, C_h \tag{7}$$

The pressure of the fluid flows as exponentially decaying transverse pressure gradient was assumed, and the dimensionless governing equations are expressed as follows.

Assuming pressure gradient by using [22]:

$$\frac{\partial P_h}{\partial x} = -e^{-\lambda t} \tag{8}$$

The equation of momentum using [34] with constant pressure coefficient, as in [32]:

$$\frac{\partial u_h}{\partial t} = p_k e^{-\lambda t} + \left(\frac{\partial^2 u_h}{\partial y^2}\right) - \sigma^2 u_h + Gr\, \theta_h + Gc\, C_h \tag{9}$$

The equation of energy using [2] with the heat conduction parameter:

$$\frac{\partial \theta_h}{\partial t} = \frac{1}{Pr}\frac{\partial^2 \theta_h}{\partial y^2} - J\theta_h \tag{10}$$

The equation of momentum using [34] with the concentration parameter:

$$\frac{\partial \phi_h}{\partial t} = \frac{1}{Sc}\frac{\partial^2 \phi_h}{\partial y^2} + k\phi_h \tag{11}$$

where

$Gr = \frac{g\beta_T(T_w{}^* - T_\infty{}^*)\nu}{U_0{}^3}$ [Grashof number];

$Gc = \frac{g\beta_{TC}(C_w{}^* - C_\infty{}^*)\nu}{U_0{}^3}$ [Mass Grashof number];

$\sigma^2 = \frac{\nu^2}{U_0{}^2 K}$ [Porosity parameter];

$Re = \frac{hu_h}{\nu}$ [Reynolds number];

$\propto^2 = \frac{\omega^* l^2}{\nu}$ [Womersely number]

$Pr = \frac{\mu C_p}{k_T}$ [Prandtl number];

$k = \frac{hk}{U_0}$ [concentration parameter];

The substitution of limit conditions are:

$$\begin{gathered} u_h = 0 \; as \; y \to \infty \\ u_h = 1 + Cos \propto^2 t \; as \; y \to 0 \\ \theta_h = 0 \; at \; y \geq 0, \phi_h = 0 \; at \; y \geq 0 \\ \theta_h = 0\,, \; \phi_h = 0 \; as \; y \to \infty \\ \theta_h = 1\,, \phi_h = 1 \; as \; y = 0 \end{gathered} \tag{12}$$

3. Method of Solution

The above set of nonlinear partial differential Equations (7)–(11) are not possible to solve in a closed form. Hence, these equations were solved analytically by using the Laplace transform method after modifying the equations as ordinary differential equations. Let us consider that the solution of CSF flow velocity as u_c, temperature as θ_c, and fluid concentration as C_c holds various parameters such as the Reynolds number, Grashof numbers for mass and heat transfer, Prandtl number, Schmidt number for mass transfer, Porosity parameter, and heat conduction parameter.

We considered the sagittal sinus and spinal cord as the outlets of CSF in this process of simulation. In reality, given that a lower amount of CSF is drained through SAS and the ventricular system, the outlets were neglected due to their low impact according to the previous studies in [16].

$$L(\theta_h) = \frac{e^{-y\sqrt{(J+s)\mathrm{Pr}}}}{s} \tag{13}$$

$$L(C_h) = \frac{e^{-y\sqrt{(\mathrm{K+s})Sc}}}{s} \tag{14}$$

$$\begin{aligned} L(u_h) = e^{-y\sqrt{(k+s)}}&\left[\frac{s}{s^2+\beta^2} - \frac{1}{k+\lambda}\left[\frac{1}{s-k} - \frac{1}{s+\lambda}\right] + \frac{Gr}{R}\left[\frac{1}{s} + \frac{1-Pr}{R-s(Pr-1)s}\right]\right] \\ &- \frac{Gm}{k}\left[\frac{1}{s} + \frac{Sc-1}{k-(Sc-1)s}\right] + \frac{1}{k+\lambda}\left[\frac{1}{s-k} - \frac{1}{s+\lambda}\right] \\ &- \frac{Gr}{R}\left[\frac{e^{-y\sqrt{Pr(s+J)}}}{s} - \frac{(1-Pr)e^{-y\sqrt{Pr(s+J)}}}{R+s(Pr-1)}\right] \\ &+ \frac{Gm}{k}\left[\frac{e^{-y\sqrt{(K+s)Sc}}}{s} - \frac{(1-Sc)e^{-y\sqrt{Sc(K+s)}}}{R+(Sc-1)s}\right] \end{aligned}$$

After solving the above Laplace equations, we obtain the velocity and the concentration equation as follows:

$$\theta_h = \frac{1}{2}\left\{\left[e^{-y\ Pr\sqrt{J}}\left[erfc\left(\eta\sqrt{Pr}\right) - \sqrt{JPrt}\right] + e^{y\ Pr\sqrt{J}}\left[erfc\left(\eta\sqrt{Pr}\right) + \sqrt{JPrt}\right]\right\} \tag{15}$$

$$C_h = \frac{1}{2}\left\{\left[e^{-y\ Sc\sqrt{k}}\left[erfc\left(\eta\sqrt{Sc}\right) - \sqrt{KSct}\right] + e^{y\ Sc\sqrt{k}}\left[erfc\left(\eta\sqrt{Sc}\right) + \sqrt{KSct}\right]\right\} \tag{16}$$

$$\begin{aligned} u_h(y) = Cos\beta&\left(t-\sqrt{s+k}\right) - \tfrac{1}{\lambda+k}e^{k(t-\sqrt{s+k})} + \tfrac{1}{k+\lambda}e^{-\lambda(t-\sqrt{s+k})} \\ &+\left[\tfrac{Gr}{R} - \tfrac{Gm}{2k}\right]\left[e^{-y\sqrt{k}}erfc\left(\eta-\sqrt{kt}\right) + e^{y\sqrt{k}}erfc\left(\eta+\sqrt{kt}\right)\right] \\ &-\tfrac{Gre^{Qt}}{2}\left[e^{-y\sqrt{Q+k}}erfc\left(\eta-\sqrt{(Q+k)t}\right) + e^{y\sqrt{Q+k}}erfc\left(\eta+\sqrt{(Q+k)t}\right)\right] \\ &-\tfrac{Gme^{-Dt}}{2k}\left[e^{-y\sqrt{k-D}}erfc\left(\eta-\sqrt{(k-D)t}\right) + e^{y\sqrt{k-D}}erfc\left(\eta+\sqrt{(k-D)t}\right)\right] \\ &+\tfrac{1}{k+\lambda}\left(e^{kt} - e^{-\lambda t}\right) \\ &-\tfrac{Gr}{2R}\left[e^{-ypr\sqrt{J}}erfc\left[\left(\eta\sqrt{Pr}\right) - \sqrt{JPrt}\right] + e^{yPr\sqrt{J}}erfc\left[\left(\eta\sqrt{Pr}\right) + \sqrt{JPrt}\right]\right] \\ &+\tfrac{Gre^{Qt}}{2R}\left[e^{-yPr\sqrt{J+Q}}erfc\left[\left(\eta\sqrt{Pr}\right) - \sqrt{(J+Q)\mathrm{Pr}t}\right]\right] \\ &+e^{yPr\sqrt{J+Q}}erfc\left[\left(\eta\sqrt{Pr}\right) + \sqrt{(J+Q)\mathrm{Pr}t}\right] \\ &+\tfrac{Gm}{2M}\left[e^{-ySc\sqrt{K}}erfc\left[\left(\eta\sqrt{Sc}\right) - \sqrt{KSct}\right] + e^{ySc\sqrt{K}}erfc\left[\left(\eta\sqrt{Sc}\right) + \sqrt{KSct}\right]\right] \\ &+\tfrac{Gme^{Dt}}{2M}\left[e^{-ySc\sqrt{K+D}}erfc\left[\left(\eta\sqrt{Sc}\right) - \sqrt{(K+D)Sct}\right]\right. \\ &\left.+e^{ySc\sqrt{K+D}}erfc\left[\left(\eta\sqrt{Sc}\right) + \sqrt{(K+D)Sct}\right]\right] \end{aligned} \tag{17}$$

$$Q = \frac{R}{pr-1},\ D = \frac{k}{Sc-1},\ \beta = \alpha^2,\ R = (J\ Pr - k),\ k = \sigma^2, \eta = \frac{y}{2\sqrt{t}}$$

Pressure of Fluid

The pressure of fluid can be depicted by using the following relation:

$$P_h = \int_0^{1+Cos\propto^2 t} u_h dt$$

The data chosen to depict the CSF disorder hydrocephalus symptoms, the method of solution by various biologist by using material properties, and other parameters, as listed in Tables 1 and 2, were used in the computations in MATLAB in the following section.

Table 2. Parameters used in the paper from various researchers.

Reynolds number	≥468.3 [15]
Darcy number	0.33 [17]
Womersley number	6.3–7.8 [16]
Grashof number for heat transfer	0.39
Grashof number for mass transfer	0.075
CSF Pressure (Hydrocephalus)	≥ 2700 [15]
Thermal Conductivity	0.63 [5]
Specific Heat Capacity	4.19 [2]
Prandtl number	0.54
Schmidt number	0.2

4. Results and Discussion

The objective of the paper was to assess the effects of the thermo-solute non-Newtonian CSF fluid, as depicted in Figures 2–13. Based on some of the data in Table 2, the analytical solutions for velocity, temperature, and concentration computed using the standard Laplace and inverse transform methods were validated by MATLAB and displayed graphically. To comprehend how the hydrocephalus model's pulsatile flow features behaved from the following graphs, plots of velocity (u_h), temperature (θ_h), and concentration (C_h) against time (t) are shown for various values of several parameters including the heat conduction parameter, Darcy permeability number, and Schmidt number. As per the MRI reports cited in [21], we used the range of CSF velocity from − 0.005 to 0.005 (m/s) for normal subjects and for the hydrocephalus case varying from − 0.015 to 0.015 (m/s). Furthermore, the range of concentration diffusivity was taken from the range between 0.1 and 1 (μm/s).

The fluid concentration fluctuation through time was illustrated. As seen in Figures 2 and 3, an increase in the Schmidt number caused a significant decrease in the concentration of solutes in the CSF. Higher Schmidt numbers imply that the solute particles diffuse more slowly in the CSF-saturated porous media since the Schmidt number correlates the relative rates of momentum and mass (molecular) diffusivity in the regime. Furthermore, in Figure 3, the concentration parameter decreases with an increase in time.

Figures 4 and 5 depict the fluctuation in CSF temperature with different Prandtl numbers throughout time. The temperature was shown to rise significantly with increasing time in different Prandtl numbers, suggesting that the hydrocephalus's thermal effects become more pronounced over time. It clarifies that changing the Prandtl number causes the thermal conduction to rise while decreasing the mass transfer. As one moves up in the pia mater space, the temperature drops off with an increase in the vertical coordinate. A strongly periodic (oscillatory) profile of the CSF flow was recorded, as seen in Figure 4. As the heat conduction parameter increased in Figure 5, a significant decrease in CSF temperature was seen (J). Furthermore, the CSF temperature increased over time. Stronger heat conduction in the temperature of the CSF domain caused the flow to slow.

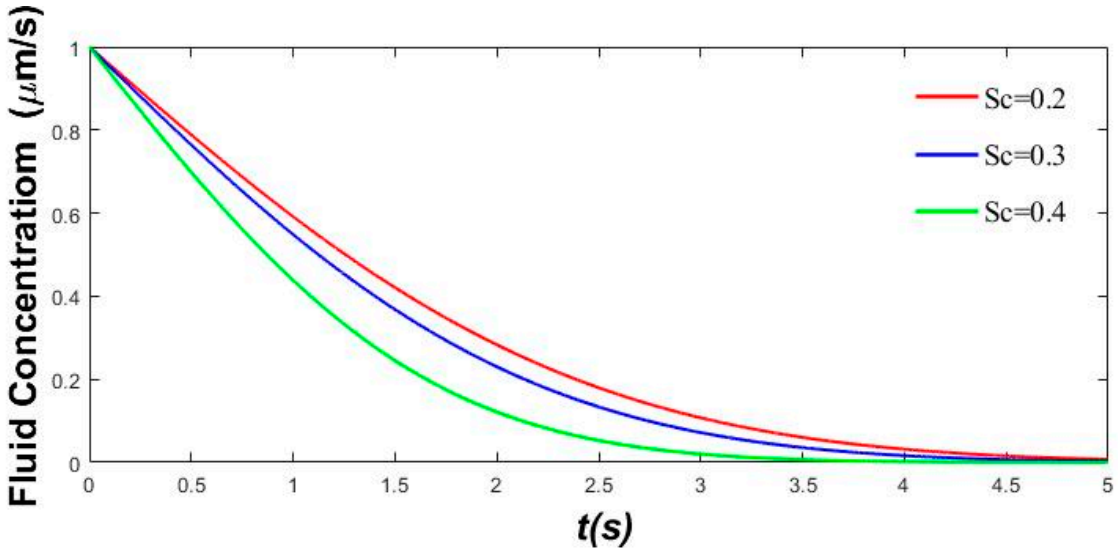

Figure 2. CSF concentration with time variation in Sc variation for hydrocephalus patients.

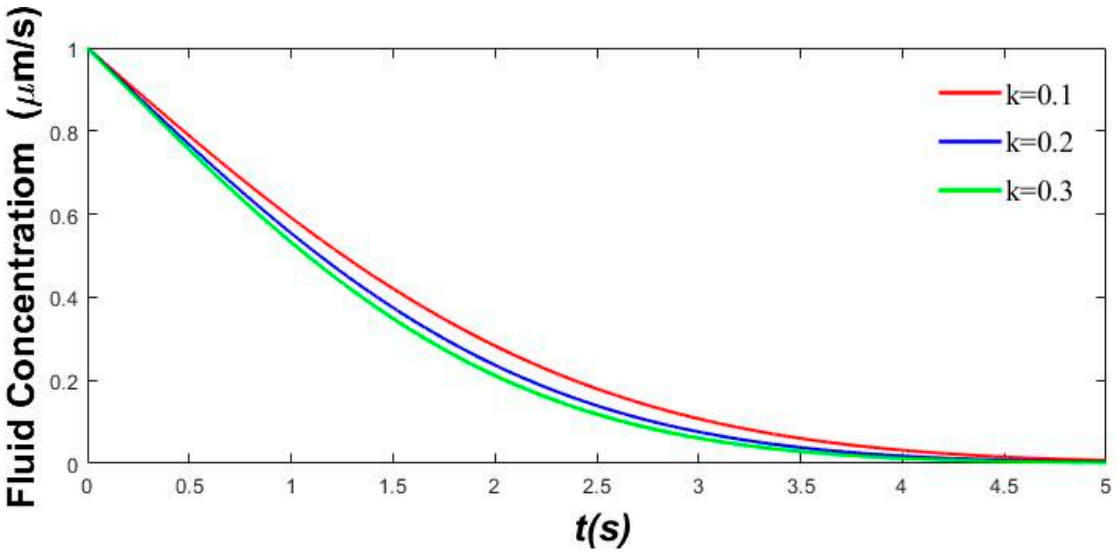

Figure 3. CSF concentration with time variation in the k variation for hydrocephalus patients.

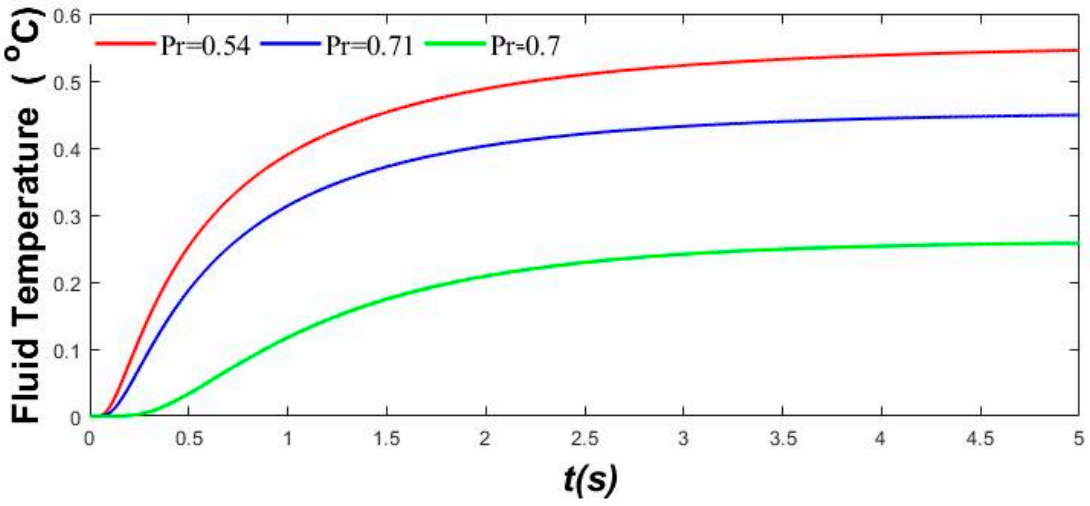

Figure 4. CSF temperature with time variation in the Pr variation for hydrocephalus patients.

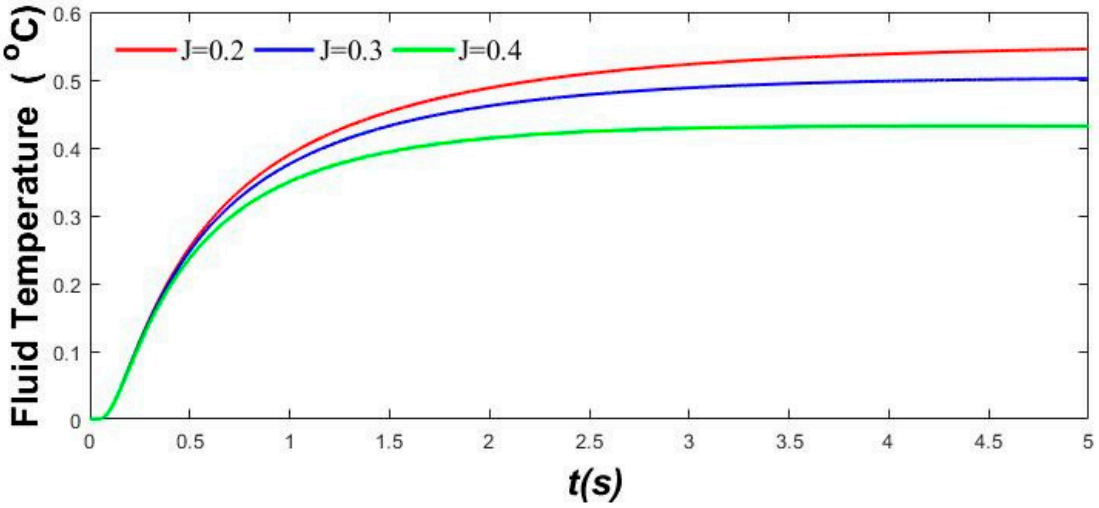

Figure 5. CSF temperature with time variation in the J variation for the hydrocephalus patients.

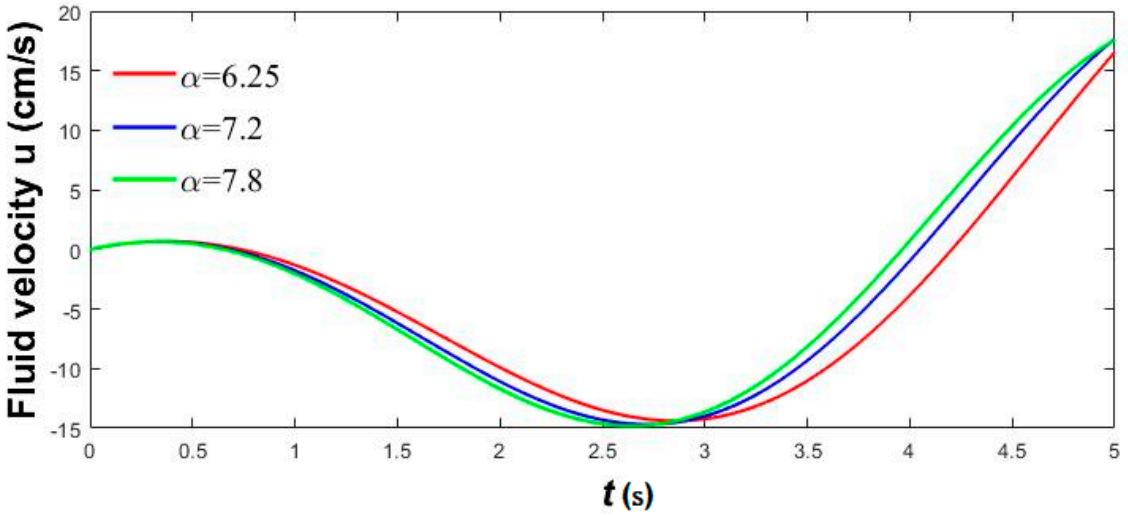

Figure 6. CSF velocity with time variation in the α variation for hydrocephalus patients.

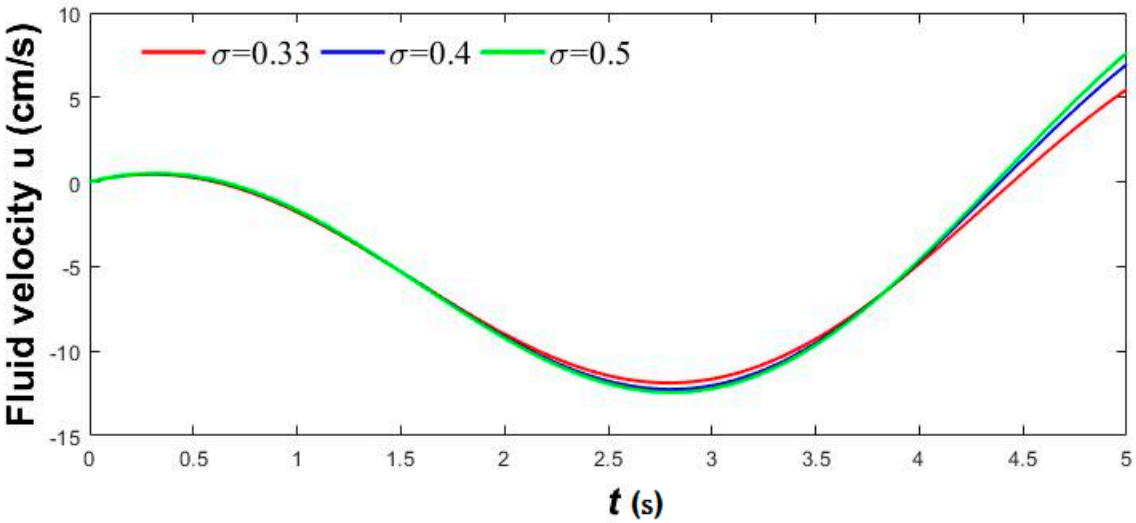

Figure 7. CSF velocity with time variation in the σ variation for hydrocephalus patients.

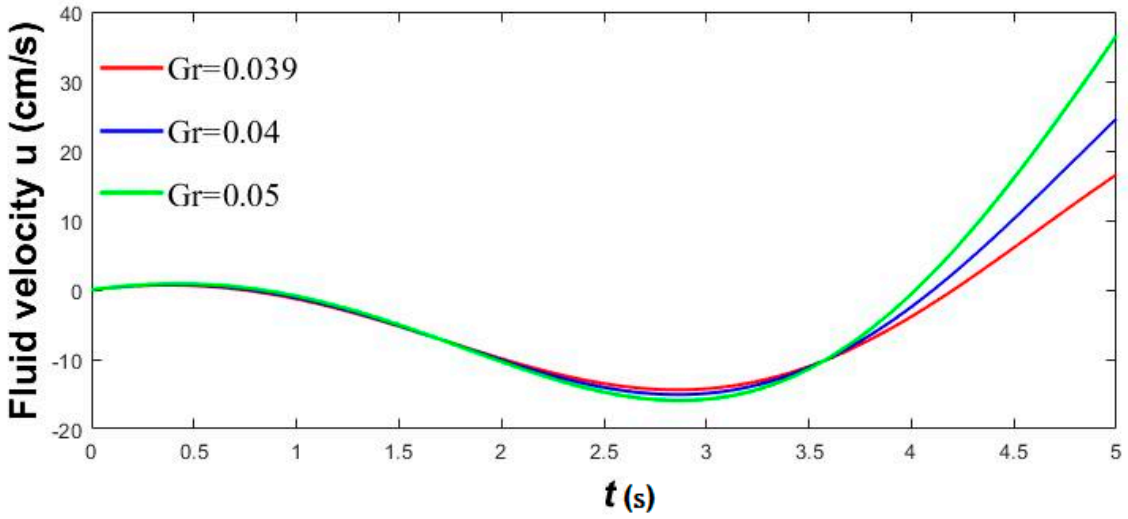

Figure 8. CSF velocity with time variation in the Gr variation for hydrocephalus patients.

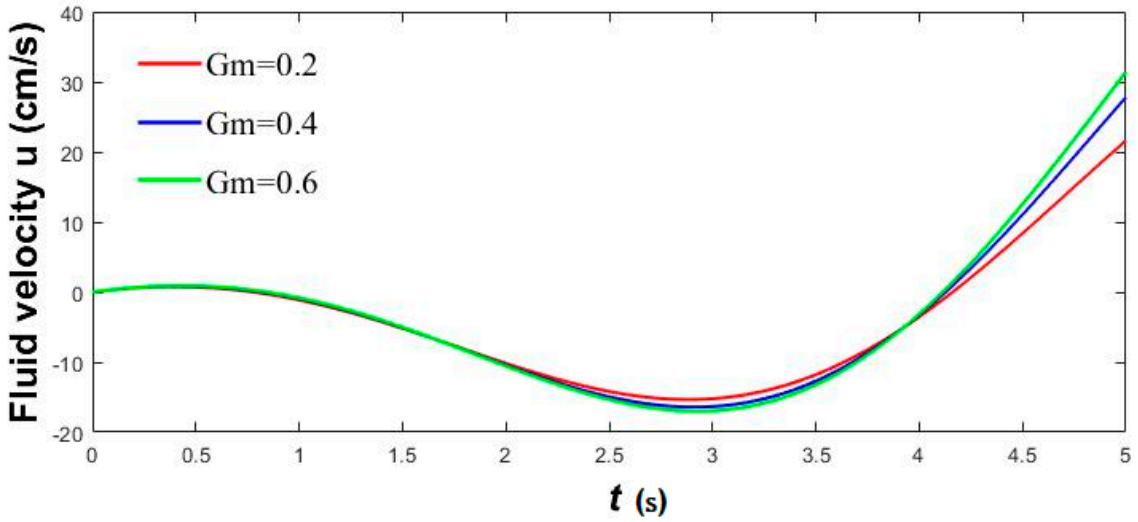

Figure 9. CSF velocity with time variation in the Gm variation for hydrocephalus patients.

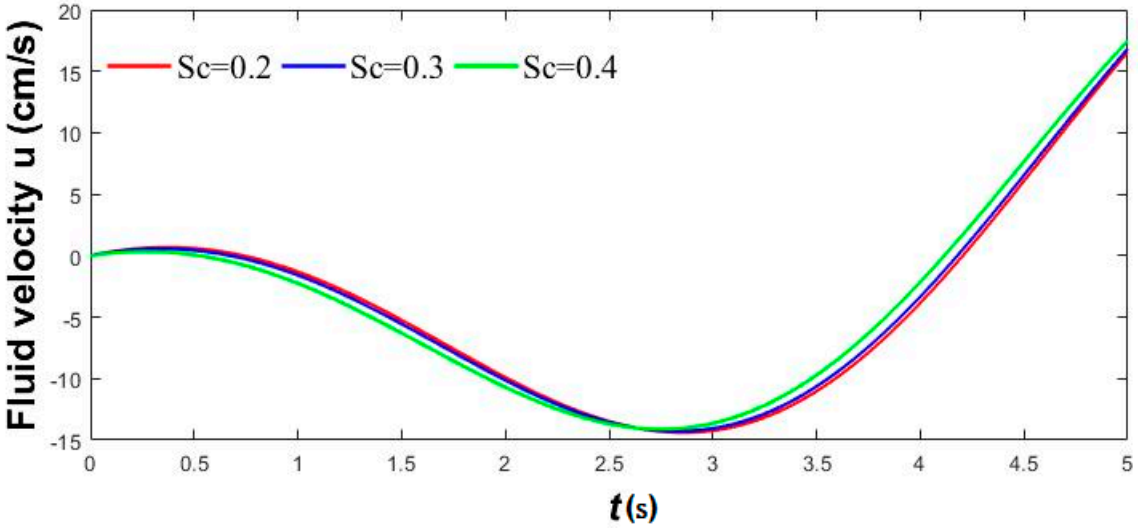

Figure 10. CSF velocity with time variation in the Sc variation for hydrocephalus patients.

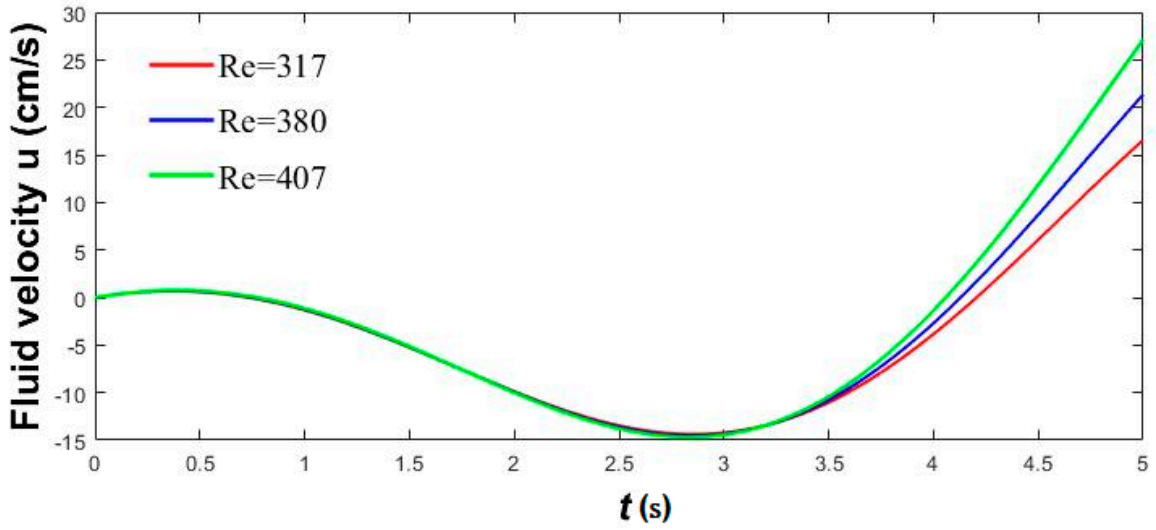

Figure 11. CSF velocity with time variation in the Re variation for hydrocephalus patients.

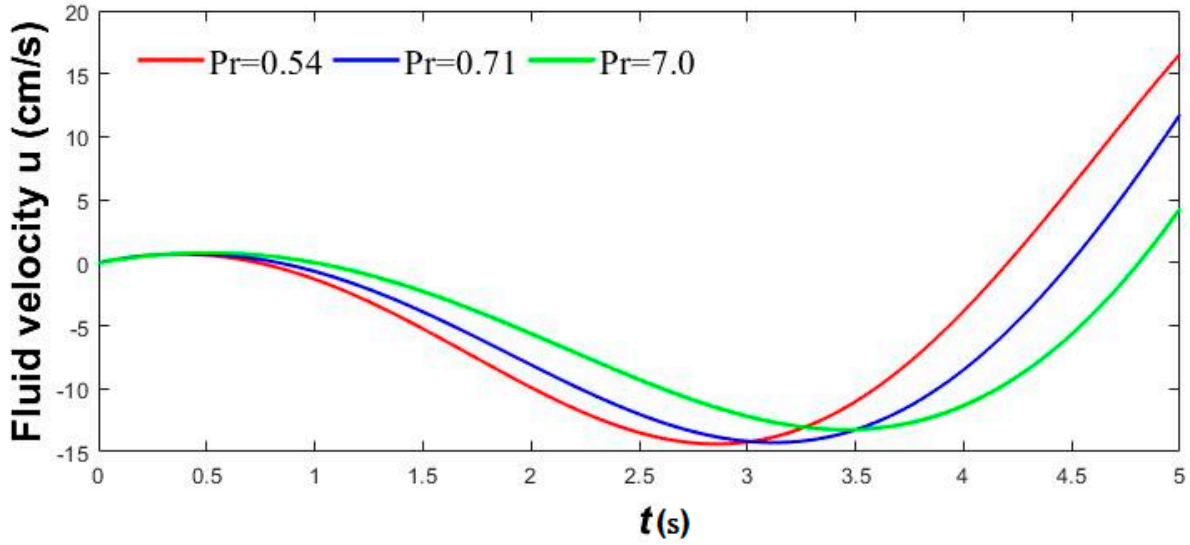

Figure 12. CSF velocity with time variation in the Pr variation for hydrocephalus patients.

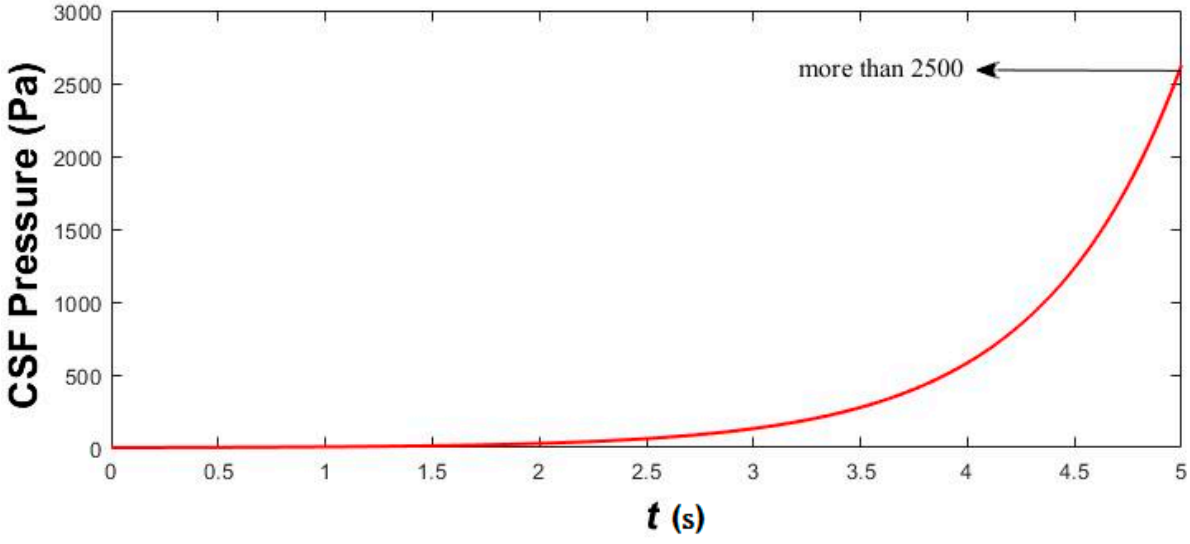

Figure 13. CSF pressure with time variation in hydrocephalus patients.

In Figure 6, the inertial force increased relative to the viscous (damping) force as the Womersley number rose. For a normal subject, the Womersley number is less than 5 and for hydrocephalic patients, it ranges from 6 to 12, as discussed statistically in [8]. The magnitudes normally stay the same, but the CSF velocity peaks and troughs (minimum values) moved as a result. Due to the periodic character of the flow, time passing seems to have had the effect of dispersing pulsatile waves. The permeability of the fluid medium increased as it retained the elasticity with respect to its length. Hence, the Darcy number decreases as the velocity of the fluid increases.

In Figure 7, it can be seen that the Darcy permeability parameter decreased the CSF velocity. The negative (drag) force that perhaps the rigid filaments in the pia mater generate on the CSF is described by the Darcian body force, $-\sigma^2 u_h$, in the dimensionless conservation of momentum equation. However, this force is inversely proportionate to the permeability, since $\sigma^2 = \frac{\nu^2}{U_0{}^2 k_m{}^*}$ The permeability clearly decreases as σ^2 rises, suggesting that the percolating CSF flow faces a higher resistance as a result. This is due to the fact that the interference in the fluid motion slows down as the size of the porous permeability increases (brain parenchyma). Hence, the fluid velocity increases in the subarachnoid space boundary layer. This change expels abnormality in the flow of CSF that affects the circulatory system.

Figures 8 and 9 show how the Grashof number affects the heat transmission and solute mass transfer, respectively. Figure 8 shows how the fluid flow significantly increases as the Grashof numbers rise, but the CSF velocities fall. On the other hand, an increase in the thermal Grashof number was used in Figure 9 to calculate the considerable reduction in CSF flow velocity. The velocity and temperature fields are coupled by Gr, which appears in the momentum equation. Higher values of Gr cause a rise in thermal buoyancy, which dampens the CSF flow regime.

The effect of the Sc parameter on the asymmetric CSF flow variations displayed with time is depicted in Figure 10. Peak displacement with time progression is evident, however, the Schmidt number has no discernible effect on the peak magnitudes.

Figure 11 depicts the variation in the Reynolds number with the time variation. The value of Re varies from 150 to 450 for hydrocephalus patients. Here, it was shown that the velocity increases when the Reynolds number escalates with time taken for the cardiac cycle.

In Figure 12, we show the influence of the Prandtl number on the time-varying CSF velocity profiles. It is known that a rise in the heat conduction parameter causes a rise in the heat diffusivity. As a result, it has been found that a rise in the Prandtl number causes a decrease in the thickness of the SAS layer due to a change in temperature. The Prandtl numbers employed in this simulation were 7.0 (water), 0.54 (CSF), and 0.71 (air), which correspond to the CSF, respectively. This is reasonable in the case where there are greater values of Pr response to the weaker thermal diffusion and thinner SAS layer.

Figure 13 demonstrates the estimated CSF pressure with a drastic elevation in normal pressure with an increase in time, which results in risk. An excess amount of fluid passes through the brain parenchyma when there is an increase in CSF pressure. As a result, the temperature, solute ions, and velocity variations in the pulsing CSF flow for the hydrocephalus subjects have been the subject of interesting observations. Strong ion diffusion in the extra fluid also contributes to the extra molecules in this pathological disease. As per the clinical reports, the CSF pressure for healthy subjects ranges up to 1015 Pa, but the hydrocephalus patient increases up to 2697 Pa [35]. Hence, the analytical methods of hydrocephalus patients in our findings resulted in more than 2500 Pa, which proved the accuracy of the clinical proof. As a result, the interaction mechanism of the intracranial fluid pressure and brain tissue is one of the controversial challenges in CNS disorders that varies with parameters such as the Reynolds number, Darcy permeability parameter, Schmidt number, Grashof number for mass and heat transfer, etc.

5. Conclusions

We evaluated the analytical method to ensure its validity before establishing the practical calculation. There is no related literature in the development of CSF mathematically to compare the numerical results with their results. As mathematicians, we developed unique rare rigorous mechanics behind CSF disorder, and justified the results with the CSF kinetics with various authors. Hence, the results of the analytical method indicate that we should pursue some recent theoretical methods by means of neurological papers. The oscillatory pressure drop with pulsatile inlet velocity was used to compare the solutions. These findings could be useful for medical researchers studying the pathological disorder of hydrocephalus. As a result, increasing the amplitude of the oscillatory velocity has no effect on improving the heat transfer of oscillating flow in a CSF heat sink. The Schmidt number parameter represents the diffusivity of the CSF flow and demonstrates that any drug injected via lumbar puncture and passed through a porous medium aid in the investigation of the current state of the human subject. As a result, every parameter exhibits some physical nature.

When there is a thermodynamical behavior regarding CSF, pulsatile inlet velocity exerts various temperature differences due to parameters such as the heat conduction parameter, and the peaks and troughs of CSF velocity are displaced as the Womersley number escalates, because the inertial force increases with relative to the dissipative force, but the magnitudes frequently remain constant. CSF pressure is essentially invariant with smaller time variations; however, after a certain time, the determined pressure significantly increases. Because of hydrocephalus dysfunction and ventricular enlargement, the subarachnoid area places a substantial amount of fluid that is passed through the brain parenchyma under intense pressure. The current study uncovered some intriguing thermosolute transport characteristics that are relevant to neurological therapy in an idealized model of hydrocephalus. The following are the findings of the current identification.

- The fluid flow velocity decreases when there are increases in the Prandtl (Pr) number, heat conduction (J) parameter, and Schmidt (Sc) number;
- As the porosity parameter, the Grashof number of heat and mass movement rises with respect to time, as does the CSF velocity;
- The temperature drops significantly when the Prandtl number and heat conduction parameter are improved;
- When the Schmidt number is increased, the fluid concentration decreases significantly;
- An upsurge in fluid velocity suggests major alterations in the flow regime's high intracranial pressure.

In order to prevent certain consequences, the patient is given suppressive therapy ahead of time. This article can be enhanced to include additional types of hydrocephalus, which would also improve the quick forecasting for real-world evaluations. The variation in the attributes of CSF amplitude as well as pressure were compared between a healthy subject approximately not more than 66.2, but in the case of the hydrocephalus patient, it was nearly twice as great as the normal subjects, as cited in Gholampour, Seifollah, et al. [34]. This paper may be helpful to approach a deep discussion into the controversial and less-known points in the brain dynamics and physio pathological kinetics. Hence, for practical use of this investigation for clinical testing enhancement, we need to expand this paper for future studies for findings with various samples.

Author Contributions: Conceptualization, H.B., N.A. and K.L.; Methodology, H.B.; Software, V.V.; Validation, V.V.; Formal analysis, N.U.R.G.; Investigation, N.A., V.V. and N.U.R.G.; Writing—original draft, H.B. and K.L.; Writing—review & editing, K.L. and N.U.R.G.; Project administration, K.L.; Funding acquisition, K.L. and N.A. All authors have read and agreed to the published version of the manuscript.

Funding: Princess Nourah Bint Abdulrahman University Researchers Supporting Project number (PNURSP2023R59), Princess Nourah Bint Abdulrahman University, Riyadh, Saudi Arabia.

Data Availability Statement: Not applicable.

Acknowledgments: We would like to thank Princess Nourah Bint Abdulrahman University Researchers Supporting Project number (PNURSP2023R59), Princess Nourah Bint Abdulrahman University, Riyadh, Saudi Arabia.

Conflicts of Interest: The authors declare no conflict of interest.

Nomenclature

CSF	*Cerebrospinal fluid*
u_h, v_h	*Dimensionless velocity of CSF flow* in x and y direction
u_h^*, v_h^*	*Dimensional velocity of CSF flow* in x^* and y^* direction
CNS	*Central nervous system*
ICP	*Intracranial pressure*
SAS	*Subarachnoid space*
ρ	*Fluid density*
ν	*Kinematic viscosity*
p_k	*Permeabilty of porous layer(pia mater)*
w_0	Characteristic velocity
α^2	*Womersely number*
λ	*Oscillating exponential parameter*
c_p	*Specific Heat capacity at constant pressure*
T_w	Pia mater wall temperature
C_w	CSF wall concentration
T_0	*CSF* steam temperature
C_0	*CSF* steam concentration
Re	*Reynolds number*
J	*Heat conduction parameter*
k'	*Thermal conductivity*
K_T	*Thermal diffusion ratio*
t	*Dimensionless time taken*
σ^2	*Darcy number*
g	*Acceleration due to gravity*
Gc	*Grashof number for mass transfer*
Gr	*Grashof number for heat transfer*
Pr	*Prandtl number*
Sc	*Schmidt number for mass transfer*
θ_h	*Temperature of fluid flow in brain*
C_h	*Transport diffusivity of the fluid*
x *and* y	*Coordinate system*

References

1. Hirashima, Y.; Takaba, M.; Endo, S.; Hayashi, N.; Yamashita, K.; Takaku, A. Intracerebral temperature in patients with hydrocephalus of varying aetiology. *J. Neurol. Neurosurg. Psychiatry* **1998**, *64*, 792–794. [CrossRef] [PubMed]
2. Sathish, R.; Qu, H.; Zakalik, K. Thermal measurement of cerebrospinal fluid flow rate in hydro-cephalus shunt. In Proceedings of the 2015 IEEE SENSORS, Busan, Republic of Korea, 1–4 November 2015; IEEE: Manhattan, NY, USA, 2015; p. 20.
3. Balasundaram, H.; Sathiamoorthy, S.; Beg, O.A. Anwar. Evaluation of the Shunt Check noninvasive thermal technique for shunt flow detection in hydro-cephalic patients. *Neurosurgery* **2011**, *68*, 198–205.
4. Neff, S. Measurement of flow of cerebrospinal fluid in shunts by transcutaneous thermal convection. *J. Neurosurg. Pediatr.* **2005**, *103*, 366–373. [CrossRef] [PubMed]
5. Herbowski; Gurgul, H. Thermodynamic Approach to Cerebrospinal Fluid Circulation. *J. Neurol. Res.* **2011**, *1*, 215–218. [CrossRef]
6. Déli, E.; Kisvárday, Z. The thermodynamic brain and the evolution of intellect: The role of mental energy. *Cogn. Neurodynamics* **2020**, *14*, 743–756. [CrossRef] [PubMed]
7. Donnelly, J.; Czosnyka, M. The thermodynamic brain. *Crit. Care* **2014**, *18*, 693. [CrossRef] [PubMed]
8. Gholampour, S.; Fatouraee, N.; Seddighi, A.S. Numerical simulation of cerebrospinal fluid hydrodynamics in the healing process of hydrocephalus patients. *J. Appl. Mech. Tech. Phys.* **2017**, *58*, 386–391. [CrossRef]
9. Zakharov, M.; Sadovsky, M. The role of blood circulatory system in thermal regulation of animals explained by entropy production analysis. *arXiv* **2013**, arXiv:1308.3663.

10. Keong, N.C.; Pena, A.; Price, S.J.; Czosnyka, M.; Czosnyka, Z.; De Vito, E.E.; Housden, C.R.; Sahakian, B.J.; Pickard, J.D. Diffusion tensor imaging profiles reveal specific neural tract distortion in normal pressure hydro-cephalus. *PLoS ONE* **2017**, *12*, e0181624. [CrossRef] [PubMed]
11. McAllister, J.P.; Williams, M.A.; Walker, M.L.; Kestle, J.R.W.; Relkin, N.R.; Anderson, A.M.; Gross, P.H.; Browd, S.R. An update on research priorities in hydrocephalus: Overview of the third National Institutes of Health-sponsored symposium "Opportunities for Hydrocephalus Research: Pathways to Better Outcomes". *J. Neurosurg.* **2015**, *123*, 1427–1438. [CrossRef]
12. Smillie, A.; Sobey, I.; Molnar, Z. A hydroelastic model of hydrocephalus. *J. Fluid Mech.* **2005**, *539*, 417–443. [CrossRef]
13. Zhu, D.C.; Xenos, M.; Linninger, A.A.; Penn, R.D. Dynamics of lateral ventricle and cerebrospinal fluid in normal and hydro-cephalic brains. *J. Magn. Reson. Imaging Off. J. Int. Soc. Magn. Reson. Med.* **2006**, *24*, 756–770. [CrossRef] [PubMed]
14. Tangen, K.M.; Hsu, Y.; Zhu, D.C.; Linninger, A.A. CNS wide simulation of flow resistance and drug transport due to spinal microanatomy. *J. Biomech.* **2015**, *48*, 2144–2154. [CrossRef] [PubMed]
15. Gholampour, S.; Fatouraee, N. Boundary conditions investigation to improve computer simulation of cere-brospinal fluid dynamics in hydrocephalus patients. *Commun. Biol.* **2021**, *4*, 1–15. [CrossRef] [PubMed]
16. Gholampour, S. FSI simulation of CSF hydrodynamic changes in a large population of non-communicating hydro-cephalus patients during treatment process with regard to their clinical symptoms. *PLoS ONE* **2018**, *13*, e0196216. [CrossRef]
17. Balasundaram, H.; Sathiamoorthy, S.; Santra, S.S.; Ali, R.; Govindan, V.; Dreglea, A.; Noeiaghdam, S. Effect of Ventricular Elasticity Due to Congenital Hydrocephalus. *Symmetry* **2021**, *13*, 2087. [CrossRef]
18. Hetnarski, R. On inverting the Laplace transforms connected with the error function. *Appl. Math.* **1964**, *7*, 399–405. [CrossRef]
19. Gholampour, S.; Fatouraee, N.; Seddighi, A.S.; Seddighi, A. Evaluating the effect of hydrocephalus cause on the manner of changes in the effective parameters and clinical symptoms of the disease. *J. Clin. Neurosci.* **2017**, *35*, 50–55. [CrossRef]
20. Seifollah, G.; Bahmani, M. Hydrodynamic comparison of shunt and endoscopic third ventricu-lostomy in adult hydrocephalus using in vitro models and fluid-structure interaction simulation. *Comput. Methods Pro-Grams Biomed.* **2021**, *204*, 106049.
21. Linninger, A.A.; Tangen, K.; Hsu, C.-Y.; Frim, D. Cerebrospinal Fluid Mechanics and Its Coupling to Cerebrovascular Dynamics. *Annu. Rev. Fluid Mech.* **2016**, *48*, 219–257. [CrossRef]
22. Sweetman, B.; Linninger, A.A. Cerebrospinal Fluid Flow Dynamics in the Central Nervous System. *Ann. Biomed. Eng.* **2011**, *39*, 484–496. [CrossRef] [PubMed]
23. Henry-Feugeas, M.C.; Idy-Peretti, I.; Baledent, O.; Cornu, P.; Lejay, H.; Bittoun, J.; Schouman-Claeys, E. Cerebrospinal fluid flow waveforms: MR analysis in chronic adult hydrocephalus. *Investig. Radiol.* **2001**, *36*, 146–154. [CrossRef] [PubMed]
24. Taylor, Z.; Miller, K. Reassessment of brain elasticity for analysis of biomechanisms of hydrocephalus. *J. Biomech.* **2004**, *37*, 1263–1269. [CrossRef] [PubMed]
25. Cheng, S.; Bilston, L.E. Computational Model of the Cerebral Ventricles in Hydrocephalus. *J. Biomech. Eng.* **2010**, *132*, 054501. [CrossRef]
26. Hochstetler, A.E.; Smith, H.M.; Preston, D.C.; Reed, M.M.; Territo, P.R.; Shim, J.W.; Fulkerson, D.; Blazer-Yost, B.L. TRPV4 antagonists ameliorate ventriculomegaly in a rat model of hydrocephalus. *J. Clin. Investig.* **2020**, *5*, e137646. [CrossRef]
27. Eide, P.K.; Brean, A. Cerebrospinal fluid pulse pressure amplitude during lumbar infusion in idiopathic normal pressure hydrocephalus can predict response to shunting. *Fluids Barriers CNS* **2010**, *7*, 5. [CrossRef]
28. Gholampour, S. Computerized biomechanical simulation of cerebrospinal fluid hydrodynamics: Challenges and opportunities. *Comput. Methods Programs Biomed.* **2021**, *200*, 105938. [CrossRef]
29. Lefever, J.A.; García, J.J.; Smith, J.H. A patient-specific, finite element model for noncommunicating hydrocephalus capable of large deformation. *J. Biomech.* **2013**, *46*, 1447–1453. [CrossRef] [PubMed]
30. Taher, M.; Gholampour, S. Effect of Ambient Temperature Changes on Blood Flow in Anterior Cerebral Artery of Patients with Skull Prosthesis. *World Neurosurg.* **2020**, *135*, e358–e365. [CrossRef]
31. Safaei, M.R.; Togun, H.; Vafai, K.; Kazi, S.N.; Badarudin, A. Investigation of Heat Transfer Enhancement in a Forward-Facing Contracting Channel Using FMWCNT Nanofluids. *Numer. Heat Transf. Part A Appl.* **2014**, *66*, 1321–1340. [CrossRef]
32. Wilkie, K.P.; Drapaca, C.S.; Sivaloganathan, S. Aging impact on brain biomechanics with applications to hydrocepha-lus. *Math. Med. Biol. A J. IMA* **2012**, *29*, 145–161. [CrossRef] [PubMed]
33. Miller, K.; Bunt, S.; Wittek, A. Computational modelling of hydrocephalus. *J. Biomech.* **2013**, *46*, 2558–2559. [CrossRef] [PubMed]
34. Balasundaram, H.; Sathiamoorthy, S.; Bég, O.A. Mathematical modeling of thermo-solutal transport in pulsating flow in the hydrocephalus. *J. Mech. Med. Biol.* **2022**, *22*, 2250071. [CrossRef]
35. Gholampour, S.; Balasundaram, H.; Thiyagarajan, P.; Droessler, J.; Yamini, B. A mathematical framework for the dynamic interaction of pulsatile blood, brain, and cerebro-spinal fluid. *Comput. Methods Programs Biomed.* **2022**, *2022*, 107209.